Wireless Breathing Sensor Based on Wearable Modulated Frequency Selective Surface

Stefano Milici, Javier Lorenzo, Antonio Lázaro, *Senior Member, IEEE,* Ramon Villarino, and David Girbau, *Senior Member, IEEE*

***Abstract*— This paper presents a wireless apnoea detector using a passive breathing sensor. The device is based on the measurement of the airflow temperature changes that are produced during breathing. The sensor is a negative temperature coefficient resistor, which is to be placed close to the nose. The functional principle is based on the change of resistance, since the body increases the temperature of the airflow, which the device receives during breathing. The wireless communication is performed using the backscattered field technique, and is based on the modulation of the response from a transponder. This backscattering technique saves a lot of energy in comparison to its alternatives and guarantees a long lifetime for the device. The transponder is composed of an array of dipoles, loaded with varactor diodes, which implement a frequency selective surface. NTC measured temperature controls the oscillation frequency of a low-frequency, two-inverter oscillator. The output of the latter modulates the varactor diodes which, in turn, modulate the backscattered response of the transponder. An algorithm, which is based on the detection of the peaks on the breathing signal in order to calculate real-time respiration and apnoea intervals, has been implemented. The reader used is also presented and experimental results are shown. The sensor can be used to perform continuous real-time measurements for long period on time due to its low-power consumption.**

***Index Terms*— Breathing sensor, frequency selective surface, wireless body area networks, wearable sensors, radio frequency identification, backscattering.**

I. Introduction

A. Background and Related Work

BREATHING is one part of physiological respiration that is required to sustain life. Unconscious breathing is controlled by specialized centers in the brain, which automatically regulate the rate and depth of breathing depending on the body need [1], [2]. The apnoea is a term for suspension of the breath. The sleep apnoea is a common respiratory disorder that occurs during sleep, which is characterized by cessations of airflow to the lungs [2], [3]. Apnoea is basically divided into two types: central and obstructive. Central apnoea is due to some deficiency on the respiratory system development, whereas the obstructive apnoea is due some type of obstruction in the airflow as shown in figure 1. This episode can occur many times during the sleep and this pathology is known as sleep-disorder breathing (SDB). The SDB is known as a relatively common condition, which can affect 24% and 9% of middle-aged men and women, respectively [1]. Apnoea events can occur 5 to 30 times an hour. Many studies have indicated that SDB is highly related to various cardiovascular diseases in forms of hypertension and stroke [2], [3]. It has also been linked to other conditions, such as: type 2 diabetes, obesity, and hypertension. The Central apnoea can't be detected by acoustic methods because it is more complicated than obstructive apnoea (OSA). In the clinical setting, the exact diagnosis is made by polysomnography (PSG) [4]. PSG measures a large number of parameters and it is made off different parts: an electroencephalogram, which records the sleep stages, a single-lead electrocardiogram, which monitors the heart rate, an electromyogram which records the leg movements, a thermal sensor and a nasal pressure transducer both of which measure the breathing rate, including airflow at the nose and at the mouth. Therefore, the PSG test is highly invasive, labor intensive,-requires expensive instruments, is a time consuming process and hence is impractical to perform apart from a general population check-up. Consequently, many people with SDB, perhaps up to 93% of the population, remain undiagnosed [5]. An effective screening in the primary core setting could increase the number of patients identified. Thus, a new generation of technological tools is under development.

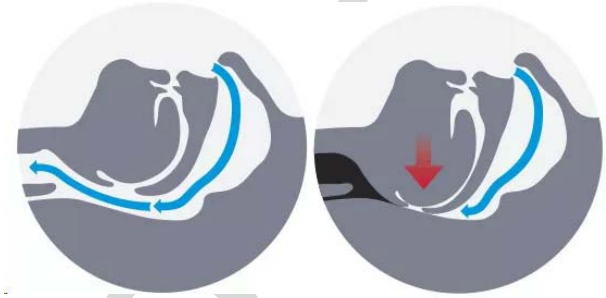

Fig. 1. Airway open during normal breathing (left) and closed airflow in an apnoea event (right).

The remote health monitoring can be acceptable in the case where the device fulfills all of the following requirements: comfortable, easy to use, and low cost. In order to detect apnea and calculate the respiration rate, there are many sensors that are commercial available. Various portable monitor devices,

Manuscript received October 29, 2016; revised December 23, 2016; accepted December 23, 2016. This work was supported in part by the Spanish Government Project under TEC2015-67883-R, in part by the H2020 Grant Agreement under Grant 645771-EMERGENT, and in part by the MiMed COST Action TD1301 under Grant BES-2012-0539802. The associate editor coordinating the review of this paper and approving it for publication was Dr. Lorenzo Lo Monte.

The authors are with the Department of Electronic, Electric and Automatic Control Engineering, Universitat Rovira i Virgili, 43007 Tarragona, Spain (e-mail: antonioramon.lazaro@urv.cat).

Digital Object Identifier 10.1109/JSEN.2016.2645766

like sleep-stripes, already exist in the market. It is an at-home sleep test diagnostic device. This device has to be worn for a minimum of five hours during sleep. The device is placed on the individual's face where the two flow sensors (oral and nasal thermistors) are placed just below the nose and above the upper lip, in order to capture the patient's breath more effectively. Most of them are based on sound recording techniques [6] or on microcontrollers which are integrated inside a belt [7]. Unfortunately, however, these devices are noisy and often, neither easy to calibrate, nor suitable for long-term monitoring.

B. Contribution and Paper Organization

In order to match the properties of comfortability, flexibility, and a long lifetime for the battery, a wireless breathing sensor that is based on a frequency selective surface (FSS) is proposed. Frequency Selective Surfaces (FSS) are periodic structures that have already been used for various applications on microwaves, optical frequency filters, radar absorbing materials (RAMs) and antenna reflectors [8]. Electronic Band Gaps (EBG) and Artificial Magnetic Conductors (AMCs), which are inspired by an FSS have often been used to reduce the size of the antennas and to mitigate the influence of the body in wearable applications [9], [10]. The viability of FSS to transmit information from the on body sensors has been shown in a recent work [11], [12]. The novelty of this work is the application of these devices as a wireless interface of the breathing sensors.

This paper is structured as follows: the sensing principle and the fundamental theory are presented in section II. Section III presents the processing of the signal that is used to estimate both the breathing rates estimation and the apnea detection. Section IV shows measurements from the prototypes. Finally, section IV draws the conclusions.

II. Sensor Design Based on FSS

A. Sensing Principle

The breathing sensor is based on a thermistor, which is placed at a certain distance from the nasal cavities and connected to an oscillator, which modulates the FSSs' response. As core body temperature is usually higher than environmental temperature, respiratory airflow increases the temperature, detected by the sensor, producing a variation of its resistance [11]. A negative temperature coefficient resistance (NTC) has been adopted as the temperature sensor. NTC is a low-priced sensor with high sensitivity in the range of the body temperature (35-41°C). A drawback of the NTC is that its resistance does not change linearly for the entire range of the measurement However, for this application, the temperature range is relatively narrow and hence a linearization can be performed. In order to avoid the usage of complex electronic circuits such as analog-to-digital converters (ADC) and microcontrollers, as well as to reduce the power consumption, an analog approach is proposed.

The oscillator is composed of two inverters based on low-voltage NANDs (SN74AUP1G00) and an RC network (see Fig.2). The resistance changes produce a frequency variation

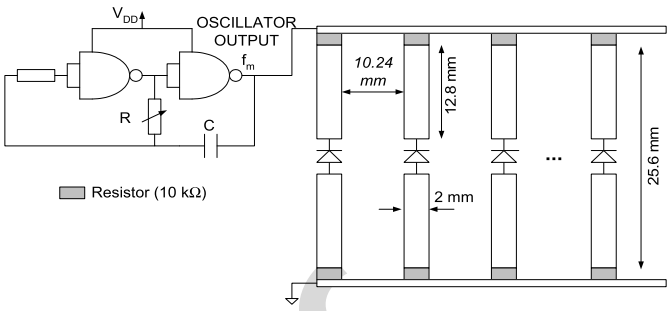

Fig. 2. Schema of a FSS loaded with varactors connected to the two-inverter oscillator controlled by the NTC resistance (R).

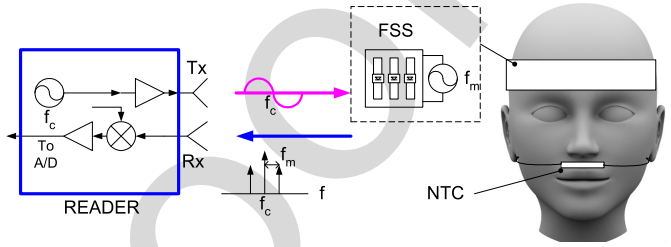

Fig. 3. Block diagram of the system, including the reader and the transponder.

at the oscillator's output that modulates the reverse-biased varactors of the FSS, which, in turn, modulates its backscattered field. The diodes are therefore switched between -3V when the output of the oscillator is in high state (3V), and 0V when the output of the oscillator is in low state (0V). The oscillation frequency can be estimated using the following expression [13]:

$$f_m = \frac{1}{2\ln(3)RC} = \frac{0.455}{RC} \tag{1}$$

where, R is the resistance of the NTC (AVX NB20R00105JBA) connected according to the schema in Fig. 2. The NTC is soldered to a thin strip of flexible PCB made with Ultralam 3850 substrate (from Rogers Corp.) and it located below the nose to detect the air flow temperature (see schema in Fig.3). The oscillation frequency depends on both the capacitance and the resistance values that are chosen in relation to the environmental temperature. In addition, these values must be adjusted taking into account both the desired frequency range allowed by the analog-to-digital converter of the reader and the Nyquist criterion to avoid aliasing. Here $C = 330$ pF produces a modulating frequency range between 2 kHz and 3 kHz around the body temperature. The Steinhart–Hart equation [14] is widely used to model the NTC resistance. The thermistor manufacturer uses the first-order approximation:

$$\frac{1}{T} \approx \frac{1}{T_0} + \frac{1}{\beta}\ln\frac{R}{R_0} \tag{2}$$

where T is the temperature in K, $R_0 = 1$ MΩ is the nominal resistance at $T_0 = 298$ K, and $\beta = 4400$ K is the Steinhart–Hart parameter that is taken from the thermistor datasheet.

The resolution in the temperature measurement is limited by the frequency resolution. Combining (1) and (2) and deriving

it as a function of the temperature, the frequency shift (Δf_m) due to the change in the temperature $\Delta T$is obtained:

$$\frac{\Delta f_m}{f_m} \approx \frac{\beta}{T} \cdot \frac{\Delta T}{T} \tag{3}$$

It should be noted that the factor β/T is very large in (3) , therefore the sensitivity in the measurement of the temperature is very high. Using signal processing techniques, a frequency resolution (Δf_m) better than 1 Hz can be achieved, as presented in the next section. Therefore, assuming a temperature value of T that is close to T_0, an oscillation frequency of 2 kHz, and a Steinhart–Hart parameter from the datasheet, the temperature resolution from the equation (3) is calculated, which is at an order of 0.01 K. For that reason this sensor can be used in several medical applications.

B. Wireless Measurement

Commercial breathing sensors [15] often use data loggers in order to store measurements, which can be processed after downloading their data onto a computer. As an alternative to those sensors, in this work, real-time wireless measurements can be performed developed. The real-time capability allows continuous monitoring of critical patients in hospitals, for which an alarm can be activated when the patient stops breathing. Since the communication is performed by a backscattering method, the transponder does not need any transmitter (e.g. Bluetooth). Furthermore, the integrated circuitry in the transponder draws low power consumption, since no ADC or microcontroller are required. Consequently, a large reduction in terms of power consumption is obtained, considering that the battery only feeds the oscillator. As a result, the battery lifetime is high even if the communication system works in continuous measurement mode. The continuous monitoring is usually performed in the case of apnoea diagnosis, where several days of analysis are required. The oscillator, based on the two-inverter that is introduced here, draws 40 μA at 3V; this leads to more than one year in the lifetime of a typical 330 mAh coin-battery. In addition, this solution allows a miniaturization of the device, as the number of parts in the system is decreased

The wireless measurement is carried out using a customized reader (details of the reader are provided below). The reader illuminates the sensor with a tone in the 2.45 GHz ISM band (f_c). The transponder backscatters the electromagnetic signal and modulates the incoming signal at the frequency of the oscillator (see fig.3), which depends on temperature.

The backscattered field (E_s) at the FSS can be expressed as a sum of two terms [11], [12], [16]: a load-independent term (structural mode) E_{est}, and a load-dependent term (antenna mode), $E_m\Gamma$.

$$\overline{E}_s = \overline{E}_{est} + \overline{E}_m\Gamma \tag{4}$$

where Γ is the complex power reflection coefficient of the diodes that load the dipoles of the FSS, which is modulated by switching the diodes using a low-frequency oscillator (with oscillation frequency f_m). Then Γ changes between $\Gamma_{\rm ON}$ and $\Gamma_{\rm OFF}$ when the diodes are in the ON state (V=0) and OFF state (V= $-$Vcc), respectively. The reflection coefficient can be approximated by a square waveform with amplitude $\Delta\Gamma = \Gamma_{\rm ON} - \Gamma_{\rm OFF}$, frequency f_m and duty cycle δ. This reflection coefficient is a periodic function that can be decomposed in a Fourier series [16]:

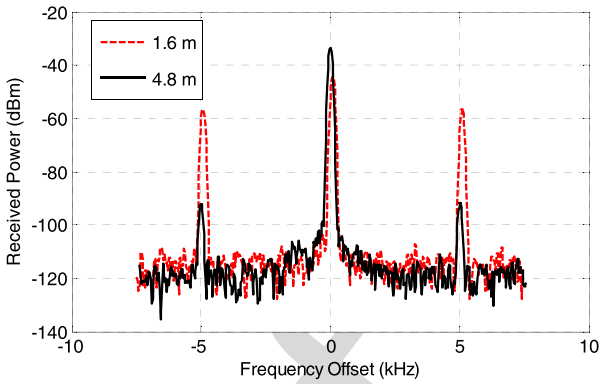

Fig. 4. Measurement of the spectrum at 2.45 GHz (at 1.6 m solid line and 4.8 m dotted line) [12].

$$\Gamma(f) = \sum_{n=-\infty}^{+\infty} c_n \delta(f - (f_c + nf_m)) \tag{5}$$

where c_n are the Fourier coefficients. For a square waveform, the backscattered field can be written using (4)-(5) as [16]:

$$\overline{E}_s = \left(\overline{E}_{est} + \overline{E}_m\Gamma_{avg}\right)\delta(f - f_c) + \overline{E}_m \sum_{n\neq 0} \Delta\Gamma\delta\left(\frac{\sin n\pi\delta}{n\pi\delta}\right)\delta[f - (f_c + nf_m)] \tag{6}$$

where $\Gamma_{\rm avg} = (\Gamma_{\rm ON} + \Gamma_{\rm OFF})/2$ are the average and difference in the power reflection coefficient between ON and OFF states, respectively.

Fig.4 shows an example of measurement of reflected power by a FSS modulated with $f_m = 5$ KHz at $f_c = 2.45$ GHz. The measurements have been done using a spectrum analyzer at two distances (1.6 m and 4.8 m). The signal received at the reader (see central peak in Fig.4) has a strong component at the center frequency (f_c) due to the structural mode of the FSS plus a constant term (see the first term in (6)) and the crosstalk between the transmitter and the receiver antennas (that doe not depends on the distance between reader and tag). The amplitude at the sidebands at $f_c \pm f_m$ (and higher-order harmonics that often fall below the noise floor of the receiver) depends on the antenna mode and decreases with the distance to the reader. Fig.4 shows that these sidebands peaks can be detected at a distance of 4.6 m. Therefore, read ranges of more than 3 m can be achieved. The FSS placed directly onto the body can achieve a large bandwidth, and the effect of losses in terms of performance, introduced by the body presence, can be compensated by increasing the number of radiating elements. The large bandwidth provides robustness to the system in front of the variation of permittivity between different bodies or the different FSS positions, considering the same body. Read ranges of around 3 m have been experimentally achieved [11], [12].

The varactor-loaded FSS is integrated in a headband along with the oscillator and the battery, as shown in Fig. 5. The NTC is connected with thin flexible wires to the oscillator to reduce the interaction with the skin, which would be more comfortable for the patient. Low-cost silicon varactors from Skyworks SMV1247-079LF are used as switching diodes. The FSS is manufactured over a 100 μm-thick Ultralam®3850 substrate. Two 10 kΩ 0605 SMD resistors are connected at the end of the arms of each dipole to feed the diodes and to prevent the undesired flow of the RF signal on the feed line. The dimensions of the FSS are provided in Fig.2. The headband is a FSS composed by four groups of 5 loaded dipoles each as shown in Fig.5. To ensure the ability to read the backscattering signal, the FSS is designed to surround the entire head and then a reading of 360° is allowed. The dipoles are also orientated in a different manner to permit the reading independently of the rotation movement of the head.

The scheme of the reader prototype is shown in Fig.6a. It has been designed using a custom software defined radio (SDR) module. The transmitter is composed by a frequency synthesizer (Minicircuits KSN-2450A-119+) that generates a signal, a Minicircuits GAL84+ to amplify it, and a linearly polarized antenna. The output power is 18 dBm. The interrogating frequency is programmed with a micro-controller (Arduino UNO board). The local oscillator for the mixer (Minicircuits LRMS-30J) that down converts the signal detected from the receiver is obtained using a coupler. The intermediate frequency (IF) signal at the mixer's output is amplified using two operational amplifiers with an overall gain of 50 dB and an analog filter with a cut-off frequency of 20 kHz connected in cascade. The output is sampled using the analog-to-digital converter (ADC) integrated in the soundcard of the PC. Fig. 6b shows a photograph of the prototype.

The sensor temperature can be determined from the modulation frequency (f_m) using (1). The modulation frequency can be obtained from the spectrum of the base band signal at the output of the mixer. The chirp Z-transform (CZT) algorithm [17], and a Hamming window is used to achieve the appropriated frequency resolution. This transform can be efficiently implemented using Fast Fourier Transforms (FFT) and makes the frequency resolution independent from the number of samples. The modulation frequency f_m is estimated from the peak of CZT using 1000 samples taken with the ADC at 44000 Hz. This procedure (sampling plus CZT and Peak detection) needs approximately 63 milliseconds. As a result, the modulation frequency that is function of the breathing is sampled at approximately 15 Hz. This sampling frequency is enough, because a normal breathing rate is around 0.3 Hz. Fig. 7 shows a sample of 20 seconds of normal respiration, taken at 1 meter of distance between the head and the reader. The samples at the output of the ADC, along with the baseband spectrum from 1.5 KHz and 3 KHz that is computed with the CZT, are shown on Fig.7.a and Fig.7.b, respectively. A clear peak corresponding to the first side-band of the modulated signal can be observed. The modulating frequency f_m can be easily obtained from the peak of the spectrum. In this case, the signal-to-noise ratio is more than 20 dB.

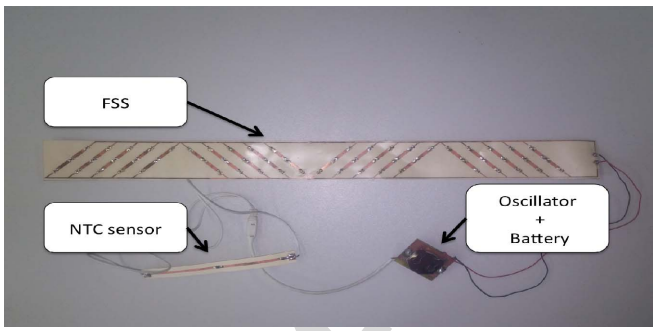

Fig. 5. Photograph of the headband with the FSS and the NTC sensor and the oscillator.

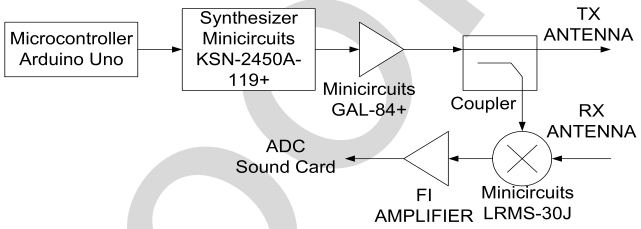

(a)

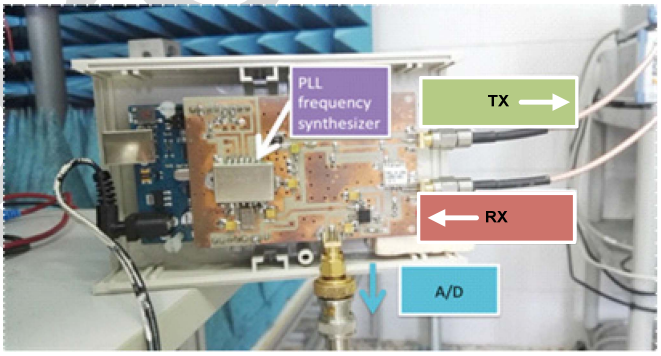

(b)

Fig. 6. Customized reader at 2.45 GHz ISM. (a) Electric scheme and photograph (b).

Fig.8 shows a histogram of the modulated frequency (sensor oscillator frequency) obtained from 5000 wireless measurements taken at room temperature (which is assumed to be constant). The measurements have been fitted using a Gaussian distribution. Fig.8 depicts the Gaussian probability distribution density overlapped to the histogram with a good agreement. The standard deviation is 1.7 Hz, which using the equation (3) corresponds to the standard temperature variation of 0.019°C. This small error due to random measurement noise does not affect this particular application.

III. Signal Processing

The block diagram in Fig.9 describes the algorithm implemented to calculate breathing rate and apnoea time. As a first step the modulating frequency f_m obtained from the spectrum of the signal, just at the output of the receiver mixer, considering it as a function of time is measured. This signal is referred to as the breathing signal.

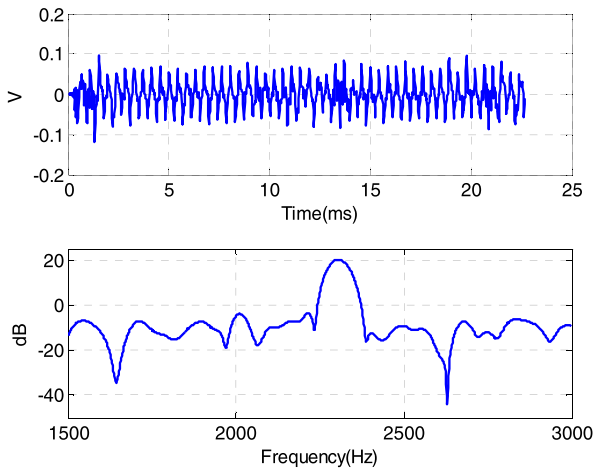

Fig. 7. Example of measurement at 1 m of distance. (a) Baseband signal in time domain. (b) Spectrum computed using CZT.

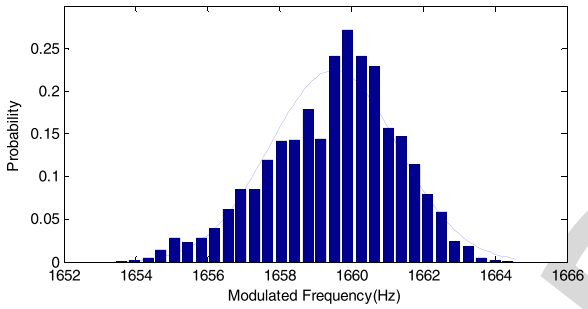

Fig. 8. Histogram and fitted Gaussian distribution of the measured modulation frequency.

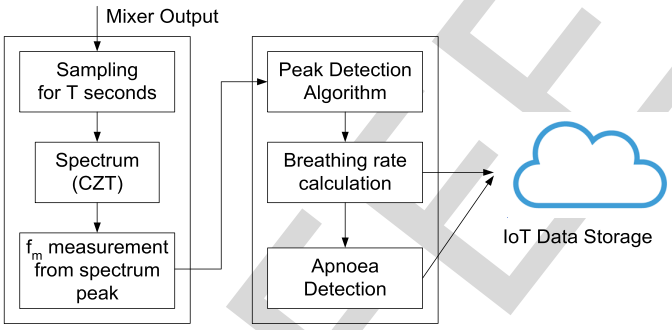

Fig. 9. Block diagram of the algorithm for breathing rate and apnoea detection.

Fig.10a shows an example of normal breathing just after installing the sensor close to the nose. It is possible to estimate the change of temperature, ΔT, in the thermistor using equation (3) from the modulated frequency shift. During the respiration cycle, the temperature variation is about 2 Kelvin when the NTC is in the vicinity of the nose. Fig.10b shows the estimated temperature change as a function of time. It can be observed that the sensor is gradually warming due to the proximity of the body, while the ripple depends on the breathing. An increase in temperature is observed during the exhalation time, and a decrease during inhalation. The amplitude of the temperature ripple depends on the relative

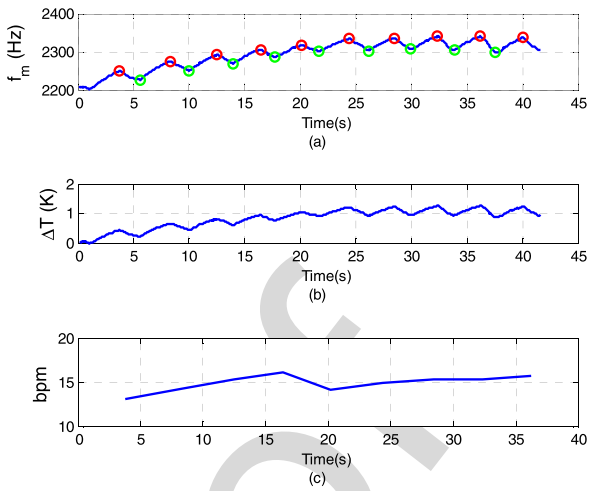

Fig. 10. Example of measurement for a person with normal breathing: (a) measured modulation frequency, (b) temperature change and (c) breathing rate in bpm as function of the time.

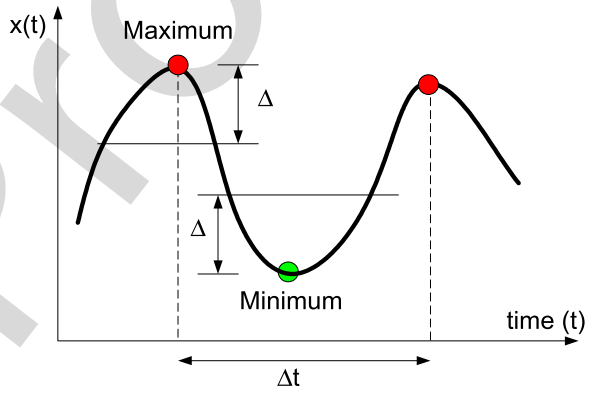

Fig. 11. Strategy to find the local maximum and minimum of the data.

distance between the sensor and the nasal cavity. A real-time peak detection algorithm has been developed to obtain the peaks and troughs of the breathing signal. Then the breathing rate, usually expressed in breaths per minute (bpm) is estimated from the inverse of the interval between two consecutive peaks, $1/\Delta t$ (fig.10c).

The algorithms to detect the local maximum (or minimum) usually present some problems in case of noisy data such as breathing data or ECG data. The well-known zero-derivative method often fails when the zero crossing of the first derivate occurs, due to noise. A typical solution consists of smoothing the curve by using different low-pass filters [18]. In this work, a robust peak detection algorithm is presented. The algorithm assumes that a peak occurs at its highest point between troughs and that there are lower points around it. The strategy is to look for the highest point and around it there are lower points shown by a Δ on both sides (see Fig.11). The algorithm only needs the current sample and the last detected maximum (or minimum). Thus, it can be efficiently implemented on quasi-real-time for continuous breathing monitoring. The pseudo code is shown in Fig.12.

```
# Initialization of variables
maximum = Inf; minimum = -Inf;
lookformax = 1

do for each measurement
{
  #Perform a measurement
  # t is the measurement instant
  # x is the measured sample

   if x > maximum
    {
     maximum = x
     maximumposition = t
    }
  if x < minimum
   {
    minimum = x
    minimumposition = t
   }

  if lookformax=1
  {
    if x < maximun-delta
    {
      save the maximun and maximum position
      minimun = x
      minimumposition = t
      lookformax = 0
    }
  }
  else
  {
    if x > minimun+delta
     {
      save the minim and minimum position
      maximun = x
      maximumposition = t
      lookformax = 1
     }
  }
}
```

Fig. 12. Pseudocode of the peak detection algorithm.

IV. Experimental Results

The prototype has been integrated into a flexible headband (see Fig.13a) in order to test the algorithm, measure the reading distance, and assess the power consumption in a real situation. The headband is placed around the head of a volunteer and the sensor is placed under the nose, as shown in Fig. 13b. The reading distance is taken standing up, in front of the reader for a period of time of 100 seconds. The maximum reading distance measured is up to 3 meters (Fig.14).

The respiration rate is calculated at the same time. Figure 15 shows the respiration fluctuation at a certain distance from the reader. Three apneas are shown with different time duration (12.4 s, 8.1 s, 9.7 s, respectively). During these time intervals, no ripple in the breathing signal is observed and the temperature decreases, gradually return to the ambient temperature. The apnea interval can be measured between a maximum and minimum when the interval (Δt) is larger than a threshold time. This threshold time is typically given as 10 seconds in the literature and it is considered as a dangerous apnoea [5]. A variation in terms of angular rotation has also been performed. The rotation of the head changes the backscattering power of the signal. Some diverse positions were considered in order to check the robustness of the system. Fig.16 shows

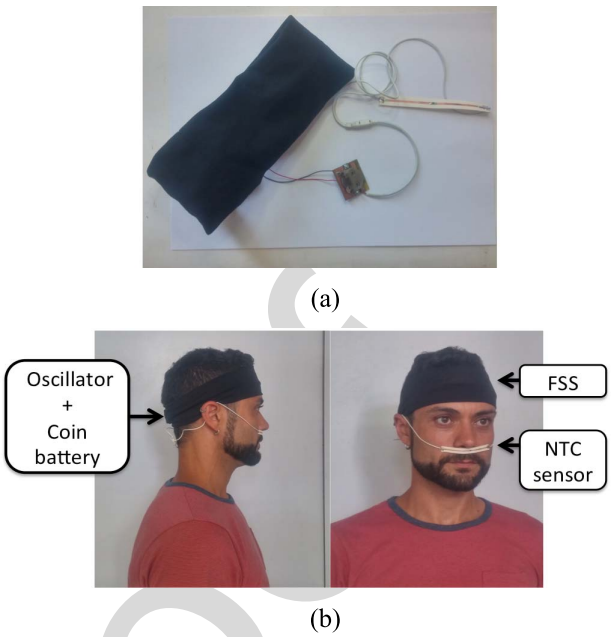

Fig. 13. Breathing sensor prototype for the measurements.

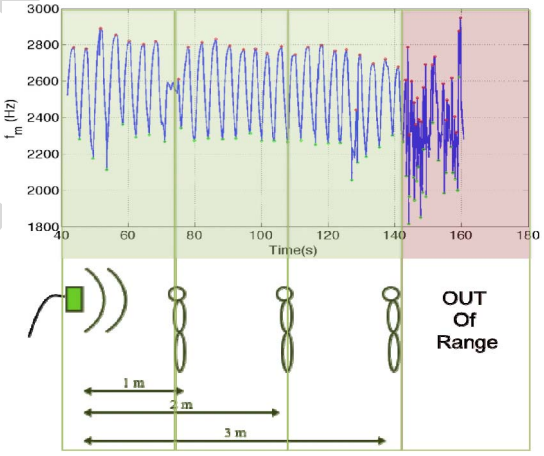

Fig. 14. Reading distance for the FSS placed on body.

the measured breathing signal for frontal and lateral head orientations. Fig.17 shows the measured breathing signal as function of the head inclination. A rotation of 90° or change in the head inclination (see Fig.17) does not affect the result, and it is correctly processed (Fig.16.c and Fig.17.c, respectively). The amplitude of the sampled signal at the output of the A/D depends on the distance to the reader (see Fig.16.a and Fig.17.a). However, the amplitude of the signal breathing (modulation frequency detected after the CZT,) depends on the frequency shift due to temperature change that is a function of the distance between the sensor, nose and the airflow velocity; to avoid this effect, a distance between the nose and the sensor is fixed. Therefore, the normalized amplitude of the signal breathing (see Fig.16.b and Fig.17.b) remains approximately constant.

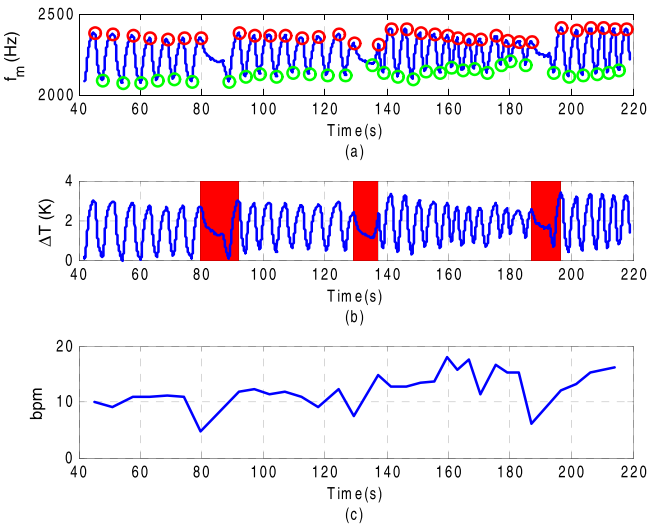

Fig. 15. Example of measurement for a person with apnoeas: (a) measured modulation frequency, (b) temperature change and (c) breathing rate in bpm as function of the time.

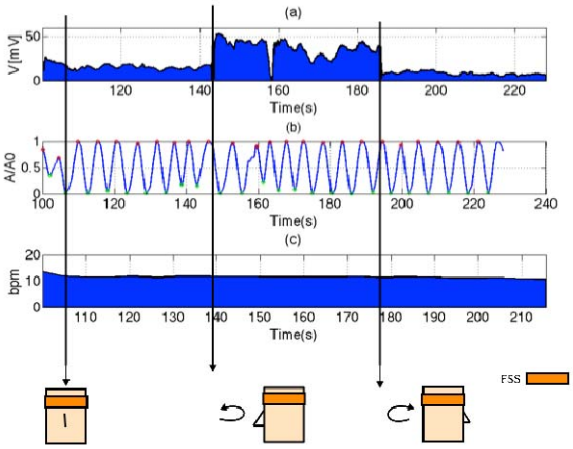

Fig. 16. Sampled signal at the output of the A/D (a), normalized breathing signal (b) and breathing rate (c) as function of time for different head rotation.

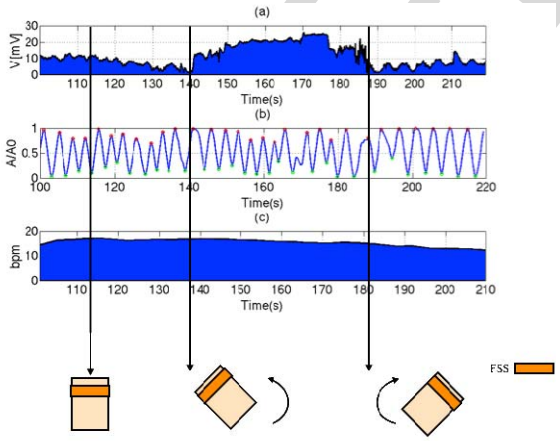

Fig. 17. Breathing sampled signal at the output of the A/D (a), normalized breathing signal (b) and breathing rate (c) for different head inclination.

V. Conclusions

This paper has presented a system for wireless breath monitoring and apnoea detection that uses transponders based on frequency selective surfaces (FSS). The communication between the transponder and the reader has been performed by the backscattering technique. The radar cross section of the FSS-based transponder is modulated using low-cost reverse-biased varactors. The power consumption of the semi-passive FSS is therefore very low compared to other alternatives. The varactors are driven by an oscillator and the frequency is controlled by a thermistor placed close to the nose cavities. The temperature at the sensor depends on the airflow during respiration. The transponder contains several FSS's with different directions and is located around the head. This topology shows high robustness in front of fadings due to non-line-of-sight (NLOS) situations, which might be caused when the path is partially blocked, either by objects or the body. A custom reader has also been developed using commercial components. Read ranges up to 3 m are typically obtained with the proof-of-concept prototype. A real time algorithm that consists of determining the respiration peak and the measured modulated frequency is used to measure the breathing rate and detect the apnoea intervals. The low power consumption enables long-term sessions of apnoea monitoring for screening applications at home. These results open the door to more complex sensors based on FSS on-body applications, which integrate microcontrollers and more sophisticated sensors for other applications.

References

[1] T. Young, M. Palta, J. Dempsey, J. Skatrud, S. Weber, and S. Badr, "The occurrence of sleep-disordered breathing among middle-aged adults," *New England J. Med.*, vol. 328, pp. 1230–1235, Apr. 1993.

[2] J. M. Parish and V. K. Somers, "Obstructive sleep apnea and cardiovascular disease," *Mayo Clin. Proc.*, vol. 79, no. 8, pp. 1036–1046, Aug. 2004.

[3] C. L. Bassetti, M. Milanova, and M. Gugger, "Sleep-disordered breathing and acute ischemic stroke," *Stroke*, vol. 37, no. 4, pp. 967–972, Apr. 2006.

[4] C. Iber, S. Ancoli-Israel, A. L. Chesson, and S. F. Quan, *The AASM Manual for the Scoring of Sleep and Associated Events*. Westchester, IL, USA: Academy, 2007.

[5] H. K. Yaggi and K. P. Strohl, "Adult obstructive sleep apnea/hypopnea syndrome: Definitions, risk factors, and pathogenesis," *Clin. Chest Med.*, vol. 31, no. 2, pp. 179–186, 2010.

[6] P. Corbishley and E. Rodriguez-Villegas, "Breathing detection: Towards a miniaturized, wearable, battery-operated monitoring system," *IEEE Trans. Biomed. Eng.*, vol. 55, no. 1, pp. 196–204, Jan. 2008.

[7] C. R. Merritt, H. T. Nagle, and E. Grant, "Textile-based capacitive sensors for respiration monitoring," *IEEE Sensors J.*, vol. 9, no. 1, pp. 71–78, Jan. 2009.

[8] B. A. Munk, *Frequency Selective Surfaces: Theory and Design*. Hoboken, NJ, USA: Wiley, 2005.

[9] S. Zhu and R. Langley, "Dual-band wearable textile antenna on an EBG substrate," *IEEE Trans. Antennas Propag.*, vol. 57, no. 4, pp. 926–935, Apr. 2009.

[10] A. Chauraya, R. Seager, W. Whittow, S. Zhang, and Y. Vardaxoglou, "Embroidered frequency selective surfaces on textiles for wearable applications," in *Proc. Antennas Propag. Conf. (LAPC)*, 2013, pp. 388–391.

[11] J. Lorenzo, A. Lazaro, R. Villarino, and D. Girbau, "Modulated frequency selective surfaces for wearable RFID and sensor applications," *IEEE Trans. Antennas Propag.*, to be published. AQ:2

[12] J. Lorenzo, A. Lazaro, D. Girbau, R. Villarino, and E. Gil, "Analysis of on-body transponders based on frequency selective surfaces," *Prog. Electromagn. Res.*, vol. 157, pp. 133–143, 2016. AQ:3

[13] *Application Note 118 CMOS Oscillators*, Fairchild Semiconductor, Sunnyvale, CA, USA.

[14] J. S. Steinhart and S. R. Hart, "Calibration curves for thermistors," *Deep Sea Res. Oceanogr. Abstracts*, vol. 15, no. 4, pp. 497–503, Aug. 1968. AQ:4

[15] (Nov. 10, 2015). *The 10 Best Sleep Trackers In 2016 Reviewed And Compared*. [Online]. Available: http://www.Nosleeplessnights.com

[16] A. Lazaro, J. Lorenzo, R. Villarino, and D. Girbau, "Backscatter tag based on frequency selective surface for FMCW radar applications," *Radioengineering*, vol. 23, no. 2, Jun. 2014.
[17] L. Rabiner, R. Schafer, and C. Rader, "The chirp Z-transform algorithm," *IEEE Trans. Audio Electroacoustics*, vol. 17, no. 2, pp. 86–92, Jun. 1969.
[18] J. Pan and W. J. Tompkins, "A real-time QRS detection algorithm," *IEEE Trans. Biomed. Eng.*, vol. 3, no. 3, pp. 230–236, Mar. 1985.

Stefano Milici received the M.Sc. degree in medical engineering from the University of Rome Tor Vergata, Rome, Italy, in 2014, where he is currently pursuing the Ph.D. degree in computer science, robotics, and electromagnetics. In 2015, he was a Visiting Researcher with the Haute Ecole d'Ingénierie et de Gestion du Canton de Vaud, Yverdon-les-Bains, Switzerland, where he was involved in research on navigation system for blind and visually impaired people. Since 2016, he has been pursuing the Ph.D. degree with the Department of Electronics, Rovira i Virgili University, Tarragona, Spain.

Javier Lorenzo was born in Reus, Spain, in 1978. He received the degree in telecommunications technical engineering and the M.S. degree in electronics engineering from Universitat Rovira i Virgili, Tarragona, Spain, in 2009 and 2011, respectively. Since 2011, he has been a Ph.D. Researcher with Universitat Rovira i Virgili. His research activities are oriented to microwave devices and systems, with an emphasis on UWB, RFIDs, and wireless sensors.

Antonio Lázaro (M'07–SM'16) was born in Lleida, Spain, in 1971. He received the M.S. and Ph.D. degrees in telecommunication engineering from the Universitat Politècnica de Catalunya (UPC), Barcelona, Spain, in 1994 and 1998, respectively. He joined the faculty of UPC, where he currently teaches a course on microwave circuits and antennas. Since 2004, he has been a Professor with the Department of Electronic Engineering, Universitat Rovira i Virgili, Tarragona, Spain. His research interests are microwave device modeling, on-wafer noise measurements, monolithic microwave integrated circuits, low phase noise oscillators, MEMS, RFID, UWB, and microwave systems.

Ramon Villarino received the degree in telecommunications technical engineering from Ramon Llull University, Barcelona, Spain, in 1994, the degree in senior telecommunications engineering from the Polytechnic University of Catalonia (UPC), Barcelona, in 2000, and the Ph.D. degree from UPC in 2004. From 2005 to 2006, he was a Research Associate with the Technological Telecommunications Center of Catalonia, Barcelona. He was with the Autonomous University of Catalonia from 2006 to 2008 as a Researcher and an Assistant Professor. Since 2009 he has been a Professor with Universitat Rovira i Virgili. His research activities are oriented to radiometry, and microwave devices and systems, based on UWB, RFIDs, and frequency selective structures using MetaMaterials.

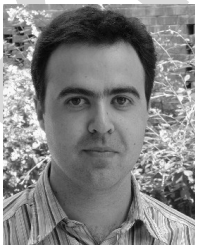

David Girbau (M'04–SM'13) received the B.S. degree in telecommunication engineering, the M.S. degree in electronics engineering, and the Ph.D. degree in telecommunication from the Universitat Politècnica de Catalunya (UPC), Barcelona, Spain, in 1998, 2002, and 2006, respectively. From 2001 to 2007, he was a Research Assistant with UPC. From 2005 to 2007, he was a part-time Assistant Professor with the Universitat Autònoma de Barcelona. Since 2007, he has been a Professor with Universitat Rovira i Virgili. His research interests include microwave devices and systems, with an emphasis on UWB, RFIDs, RF-MEMS, and wireless sensors.

AUTHOR QUERIES

AUTHOR PLEASE ANSWER ALL QUERIES

PLEASE NOTE: We cannot accept new source files as corrections for your paper. If possible, please annotate the PDF proof we have sent you with your corrections and upload it via the Author Gateway. Alternatively, you may send us your corrections in list format. You may also upload revised graphics via the Author Gateway.

AQ:1 = Please confirm whether the edits made in the financial section are ok.
AQ:2 = Please provide the volume no., issue no., page range, month, and year for ref. [11].
AQ:3 = Please provide the issue no. or month for ref. [12].
AQ:4 = Please provide the year for ref. [13].
AQ:5 = Please provide the page range for ref. [16].
AQ:6 = Please confirm whether the edits made in the sentence "Ramon Villarino received the degree in telecommunications…" are OK.